

1973

# The Investigation of Snowfall Rate Using Optical Techniques

Gerald J. Mulvey

*University at Albany, State University of New York*

Follow this and additional works at: [http://scholarsarchive.library.albany.edu/cas\\_daes\\_etd](http://scholarsarchive.library.albany.edu/cas_daes_etd)

 Part of the [Atmospheric Sciences Commons](#), [Environmental Sciences Commons](#), and the [Meteorology Commons](#)

---

## Recommended Citation

Mulvey, Gerald J., "The Investigation of Snowfall Rate Using Optical Techniques" (1973). *Atmospheric and Environmental Sciences Theses and Dissertations*. 1.

[http://scholarsarchive.library.albany.edu/cas\\_daes\\_etd/1](http://scholarsarchive.library.albany.edu/cas_daes_etd/1)

This Thesis is brought to you for free and open access by the Atmospheric and Environmental Sciences at Scholars Archive. It has been accepted for inclusion in Atmospheric and Environmental Sciences Theses and Dissertations by an authorized administrator of Scholars Archive. For more information, please contact [scholarsarchive@albany.edu](mailto:scholarsarchive@albany.edu).

The Investigation of Snowfall Rate  
Using Optical Techniques

A thesis presented to the Faculty  
of the State University of New York  
at Albany  
in partial fulfillment of the requirements  
for the degree of Master of Science

Gerald J. Mulvey  
1973

#### ACKNOWLEDGMENTS

The author wishes to express his appreciation to Associate Professor James E. Jiusto for his guidance during the year and a half while this study was in progress. He is also grateful to Dr. G. Garland Lala for his aid and guidance in developing the instruments used, and to Associate Professor Duncan Blanchard for his critical review of this thesis. In addition, he wishes to thank his wife, Katherine, for editing and typing the manuscript.

The research was conducted with support from NOAA, grant number 04-3-022-17, U. S. Department of Commerce.

## TABLE OF CONTENTS

	Page
Acknowledgments .....	(i)
List of Tables .....	(iv)
List of Figures .....	(v)
<b>1. INTRODUCTION</b>	
1.1 General statement of the problem .....	1
1.2 Specific scope of the thesis .....	5
<b>2. PROCEDURE OF THE INVESTIGATION</b>	
2.1 Experimental set-up .....	6
<b>3. INSTRUMENTS</b>	
3.1 Transmissometer .....	7
3.2 Visibility meter .....	9
3.3 Precipitation network .....	9
3.4 Precipitating particle characteristics .....	11
<b>4. DATA ANALYSIS</b>	
4.1 Transmissometer snow data .....	14
4.2 Rain data .....	15
<b>5. PRECIPITATION CHARACTERISTICS</b>	
5.1 February 16, 1973 snow characteristics .....	18
5.2 February 22, 1973 snow characteristics .....	19
<b>6. DISCUSSION</b>	
6.1 February 16 storm .....	22
6.2 February 21-22 storm .....	24
6.3 Sample volume .....	28
6.4 Spring and summer rain .....	29
<b>7. ERROR ANALYSIS</b> .....	32
<b>8. CONCLUSIONS</b> .....	33
<b>REFERENCES</b> .....	37
<b>APPENDIX</b>	
I List of symbols .....	40
II Output voltage to light intensity conversion .....	42
III Theory of attenuation .....	45

LIST OF FIGURES

	Page
FIGURE 1 Transmissometer and human eye spectral response characteristics .....	8
2 Physical set-up of experiment .....	10
3 Snow crystal camera .....	12
4 Sample computer output .....	16
5 February 16 visibility variation .....	23
6 February 21-22 visibility variation .....	27
7 Observed and calculated rainfall rates .....	30
8 Summary of observed vs. calculated rainfall rates .....	31
9 Snowfall rate vs. attenuation coefficient relationship (summary) .....	34

## INTRODUCTION

### 1.1 General

Experiments involving the attenuation of light by falling snow, or hydrometeors in general, lend themselves to the study of at least two problems of meteorological interest. The first problem is that of visibility in adverse weather conditions, and the second is that of finding a better method to measure precipitation. From the late 1940's through the late 1960's, various investigators have attempted to apply forward light scattering theory in the geometric optics range ( $\alpha \geq 200$ , where  $\alpha = \frac{2\pi r}{\lambda}$ ,  $\lambda$  = wavelength and  $r$  = radius)\* to quantitatively describe the attenuation of a light beam, and thereby visibility changes due to hydrometeors.

Recent attention has been focused on the attenuation-precipitation relationships by a series of experiments carried out in the northeast by O'Brien (1970), and in southeast Canada by Lillesaeter (1965), and by Warner and Gunn (1969). These experimental investigations were primarily aimed at measuring attenuation of a light beam due to frozen precipitation. For rain, both experimental and theoretical investigations have been carried out by various authors. Atlas (1953) partially summarized these rainfall investigations. He also developed a visibility-rainfall rate relationship from the fact that the extinction coefficient can be expressed as the sum of the effective scattering cross sections at large  $\alpha$ , and as a function of several other

---

\*Note: All symbols are defined in Appendix I.



relationships. The first of these is the Koschmieder (1924) meteorological range (V) definition ( $V = \frac{3.9}{\sigma}$ , where  $\sigma$  is the extinction coefficient). The second is the visibility relationship of aufm Kampe and Weickmann (1952), which has been adjusted for a threshold contrast ( $\epsilon$ ) of 0.055 used by Atlas:

$$V = 1.93 (\rho/W) \left( \frac{\sum_{i=1}^n N_i r_i^3}{\sum_{i=1}^n N_i r_i^2} \right)$$

where W is the liquid water content per unit volume,  $\rho$  is the density of the scattering material, and  $N_i$  is the number of drops in the  $i^{\text{th}}$  category, with a radius of  $r_i$ . The last of these relationships is the Marshall-Palmer (1948) dropsize and liquid water content expressions,  $D_0 = 0.92R^{0.21}$  and  $W = 72R^{0.88}$ , where  $D_0$  is the median volume diameter and R is the rainfall rate. The theoretical relationship arrived at by combining these expressions is  $V = 9.3R^{-0.67}$  and the empirically adjusted relationship (for Bergeron type rain) is  $V = 11.6R^{-0.63}$ . Atlas' expression differs somewhat from the similar Middleton (1952) visibility expression (p. 122), and is easier to apply.

During the 1965 and 1966 winter seasons at Lebanon Regional Airport, N.H., O'Brien (1970) attempted to use a Duntley (Scripps Institution) attenuation meter with a 91.4 cm sample pathlength to measure attenuation coefficient (visibility), and snow crystal or flake concentration. Unfortunately, over several snowstorms, an electronic failure occurred in one photometer which relegated this instrument to only a trend indicator. The visibility measurements used by O'Brien were of meteorological range with a threshold contrast  $\epsilon$  of 0.02, where  $\epsilon$  is defined as  $\epsilon \equiv \frac{\Delta B}{B}$  (Middleton, 1952, p. 87). He made no

attempt to calculate attenuation coefficients from these measurements. His attenuation coefficients were derived from scattering area concentrations which resulted in a theoretical approach to the problems in terms of an attenuation-area concentration relationship, and a mass flux-extinction coefficient relationship.

During the early 1964 winter season in Montreal, a specially constructed optical system with a 123 m base line and a  $1.13 \text{ m}^3$  cylindrical sample volume was used by Lillesaeter (1965) to make light attenuation measurements in falling snow. His light source was a broad spectrum stroboscope ( $\lambda$  center =  $0.47\mu$ ). His results showed a maximum attenuation of  $100 \text{ db km}^{-1}$  and an attenuation-snowfall rate proportionality of  $18 \text{ db km}^{-1}/\text{mmw hr}^{-1}$  for his 75 hours of data time and 49 mm of total melt water. These measurements, however, included attenuation produced by fog and pollution at the time of measurement. The attenuation by fog was said not to introduce any difficulty, while the attenuation by pollution was reported to reach a maximum of  $8 \text{ db km}^{-1}$ , and averaged  $1.5 \text{ db km}^{-1}$ . The instrument also suffered from thermal inhomogeneities in the air, caused by transmitter room-atmosphere temperature differences. The signal change was on the order of  $0.5 - 1.0 \text{ db}$  (equivalent to  $4.1 - 8.1 \text{ db km}^{-1}$ ). Due to the coarse time resolution and evaporation losses of the heated tipping bucket precipitation gauge, Lillesaeter could not establish his results with precision. His experiments were extended to include two rain showers at the end of the winter season. These showed an attenuation-precipitation rate proportionality of  $(0.25 \text{ db km}^{-1})/(\text{mm hr}^{-1})$ . This attenuation falls within the range of values in rain calculated by Atlas to be  $0.20$  to  $0.28 \text{ (db km}^{-1})/(\text{mm hr}^{-1})$ .



Warner and Gunn (1969) continued with Lillesaeter's equipment to investigate the optical attenuation of a light beam by snowfall. However, they modified the equipment by decreasing the base line to 71 meters and mounting the transmitter outdoors. This decreased the sample volume to  $0.6 \text{ m}^3$ . Their calculations showed that this volume is sufficient to contain  $10^3$  particles at a snowfall rate of about  $0.1 \text{ mmw hr}^{-1}$ , and more than  $10^4$  particles at higher rates. These experiments, which were carried out on the McGill campus in Montreal during the 1966-67 winter season, included some 20 storms with a total of 160 mm of melt water. The attenuation-snowfall rate proportionality was determined to be  $11 \text{ (db km}^{-1})/(\text{mmw hr}^{-1})$ . For 50% of all snowfall hours, the attenuation coefficient was  $4.2 \text{ db km}^{-1}$  ( $R < .38 \text{ mmw hr}^{-1}$ ) and half of the total snowfall ( $R < 1.2 \text{ mmw hr}^{-1}$ ) gave an attenuation coefficient of  $13.3 \text{ db km}^{-1}$ . The precipitation gauge performance was termed "variable" as the thermostat was being adjusted during the data-taking period. On at least one occasion, steam was observed rising from the heated funnel. The supplemental precipitation gauge was a four-inch diameter can mounted 6 feet above the surface with a Nipher wind shield. These gauges were approximately 18 m below and 50 m away from the sample volume. Humidity effects on the hygroscopic condensation nuclei of the experimental urban environment caused a 4-5  $\text{db km}^{-1}$  attenuation. This led to a possible -4 and +2  $\text{db km}^{-1}$  attenuation error, as clean air (i.e., precipitation free) attenuation during the storms was unknown.

Despite the instrumental difficulties encountered, the simple visibility-attenuation results obtained (relatively independent of snowfall type) made it attractive that more definitive experiments be

conducted in other locations to confirm or adjust the McGill findings. Such a series of experiments was undertaken during the early 1973 winter season at the State University of New York at Albany. The aim of these experiments was to develop a precipitation rate-attenuation coefficient relationship for snow by use of a local precipitation network, sheltered visibility meter, and a 117.5 m baseline transmissometer. These experiments were carried out in terms of photometric theory, that is, the visible spectrum, in contrast to the other wavelengths associated with radiometric theory.

Of the winter data collected, only 17 hours of data (1.5 mmw) proved reliable enough for data analysis. The experiments were extended to spring and early summer rains, but instrumental problems which bear on the feasibility of such a technique continued to limit the results. Alternately, visibility and precipitation data from the nearby National Weather Service Station at Albany Airport were analyzed to examine the rainfall rate-visibility relationship.

## 1.2 Specific scope of thesis

In summary, the specific objectives of this thesis were to:

1. develop a relationship between precipitation rate and attenuation coefficient, taking into consideration snow crystal type;
2. investigate the importance of sample volume when determining meteorological range and precipitation rate optically;
3. compare the rainfall rate calculated from the meteorological range and from the observed rainfall rate.



## 2. Procedure of the Investigation

### 2.1 Experimental set-up

For the purpose of measuring light attenuation and visibility, a transmissometer was constructed and set up on the roof of the Fine Arts and Earth Science buildings at the northeast end of the academic podium of the University campus. The transmitter-receiver orientation was WNW to ESE with a base line which measured  $117.5 \pm 0.5$  m in length. The light beam center line was approximately 1.3 m above roof level and 10 m above ground level. The light beam itself was inclined downward slightly from the transmitter. Its sample volume, calculated in the same way as Warner and Gunn's volume, namely, a cylinder defined by the aperture of the receiver and the pathlength, was  $1.21 \text{ m}^3$ . The geometry of the beam was roughly that of a frustum of a cone. It started out as a 30.5 cm diameter circular beam and diverged to a roughly circular beam approximately 400 cm in diameter. The lower portion of this cone was blocked somewhat by the intervening section of the roof. The beam was allowed to broaden in such a fashion to allow for vibration of the receiver and transmitter due to wind. The sample volume traversed a path over two open sections of the roof separated by a 6 m wide section of roof. It was high enough above ground to eliminate blowing snow from the ground. However, blowing snow from the rooftop was observed to cross the optical path several times during the experiments. These cases did not cause difficulty because of their transitory nature and the averaging techniques used in the data reduction.

### 3. Instruments

#### 3.1 Transmissometer

The light source of the transmissometer was a modified 12 inch diameter Navy signaling search light. It consisted of the housing, parabolic mirror and shutter assembly from the search light, and an 18 ampere 6 volt CPG G.E. incandescent projection lamp for its source. The projection lamp had a broad spectrum with a color temperature of  $3075^{\circ}$  K ( $\lambda_{\max} = 9100\text{\AA}$ ). The shutter was closed automatically by a rotary solenoid for 10 seconds out of every 60 seconds to permit background light level measurement. The receiver consisted of a 4 1/2 inch reflecting telescope and a 120X power eyepiece to collect and focus the incoming beam. Both the transmitter and receiver were on the open roof away from any heated structures. Due to restrictions on the type of mounting for the transmissometer, it was necessary to use cinder blocks and ropes to weigh down and secure the instrument. The transmitter was contained in its own housing and supported by a pillar mount. The receiver was mounted in an unheated wooden housing which was supported approximately 1 m above the roof. The housing was designed to permit free air circulation around the telescope to minimize the risk of mirror and optics fogging up. The detector itself consisted of a narrow band pass filter ( $\lambda_{\max} = 5250\text{\AA}$ ) and a photoresistor. These were both carefully selected to simulate the average response of the human eye, as shown in Figure 1. The photoresistor acted as a feedback control resistor on a Fairchild frequency compensated operational amplifier (model  $\mu$ A741). This voltage was then transmitted to a



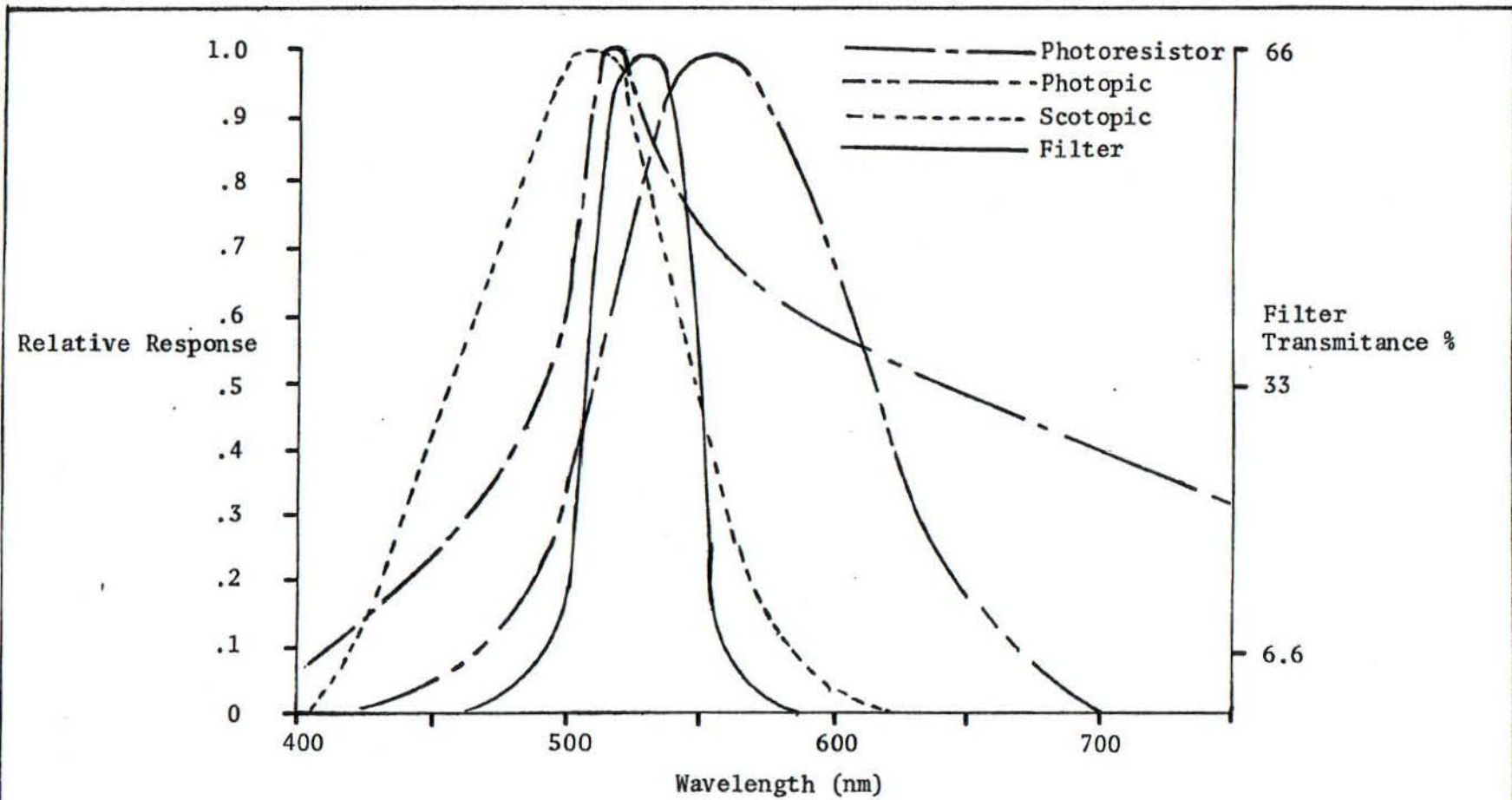


**Fig I** Spectral Response Characteristics

Hewlett Packard strip chart recorder, where it was recorded along with the "clear air" visibility,\* (i.e., free of snow or rain).

### 3.2 Visibility meter

An AEG/Telefunken light scattering meter was used to measure clear air visibility. This light scattering meter was positioned between 2 unheated small sheds on the roof, and was sheltered under a tarpaulin to prevent snow crystals or raindrops from entering the sampling volume while allowing free air ventilation. Its scattering volume is  $7.9 \times 10^{-4} \text{ m}^3$ .

### 3.3 Precipitation network

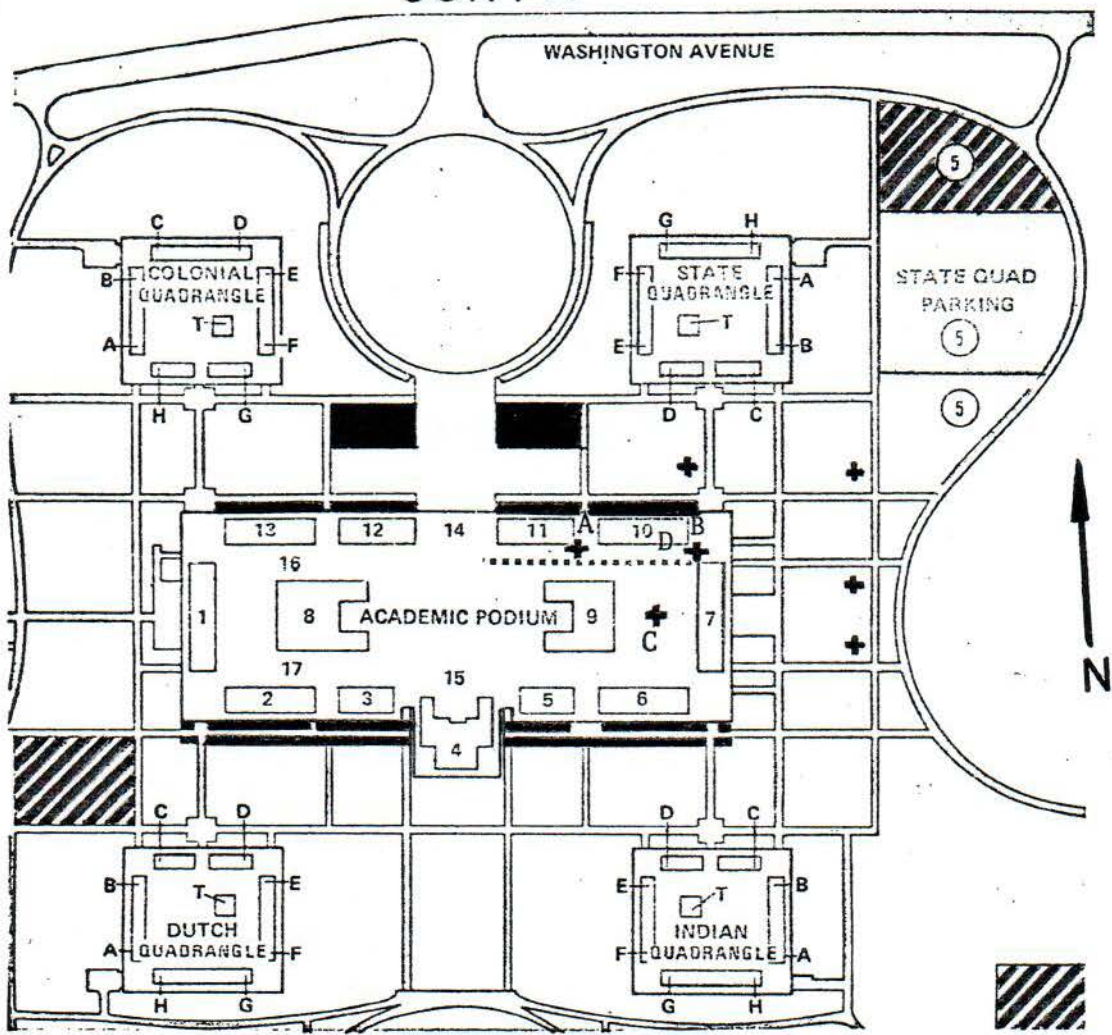
The precipitation network consisted of 2 weighing buckets and 2 heated tipping buckets all shielded by Alter windshields. The two weighing buckets were positioned on the open roof approximately 10 m NNE of the transmissometer sample volume. Weighing bucket number one was positioned 5 m behind the receiver, and number two was positioned roughly halfway between the transmitter and receiver. One of the heated tipping buckets was positioned next to weighing bucket number one; the other heated tipping bucket was placed in the middle of a garden area surrounded by four podium buildings all approximately 10 m high, with connected roofs. The opening above the garden tipping bucket was approximately 95 m by 50 m. The instrument positions are shown in Figure 2.

In addition to this, a snow sample station line was operated during the winter. It consisted of 5 snow board stations marked by

---

\*For details of output voltage to light intensity conversion see Appendix II.

# SUNY-A





-  Transmissometer baseline (117.5m)
-  Precipitation measurement sites
- 11 Fine Arts building
- 10 Earth Science building

Fig 2 Physical Setup



white poles, all of which were located N and E of the transmissometer. At each station, snow depth was measured every 3 hours. New snow accumulation was measured at three stations and total accumulation was measured at two stations.

#### 3.4 Precipitating particle characteristics

Some of the physical characteristics of the precipitating particles were measured on the roof at various points throughout the storms. This was done to investigate the dependence of attenuation on snow crystal type, as noted but not examined in detail by Warner and Gunn (1969, p. 121). For the winter sample period the snow crystal type was determined. A snow crystal camera was developed for this purpose. As sketched in Figure 3 this device consisted of a Bolex H 16 movie camera, operating on single frame exposure, and a motorized felt belt. The exposure time of the belt itself to the falling snow could be varied. This could be done at the investigator's discretion by varying the speed of the moving belt. The crystals captured would then be cooled by dry ice trays under the belt until they reached the photographing area, where a photoelectric trigger would simultaneously fire an electronic strobe and open the camera shutter. The snow was then removed from the belt, and the belt was prepared for another exposure. The continuous permanent record of snow crystal type could then be subsequently analyzed.

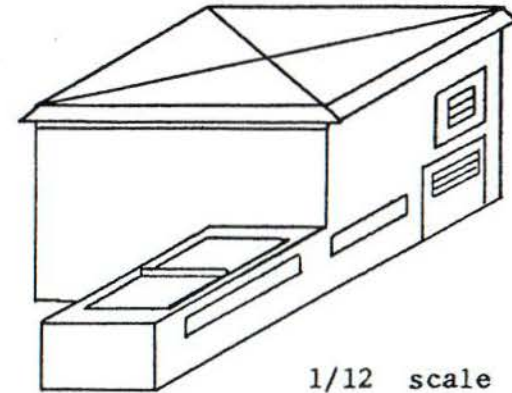
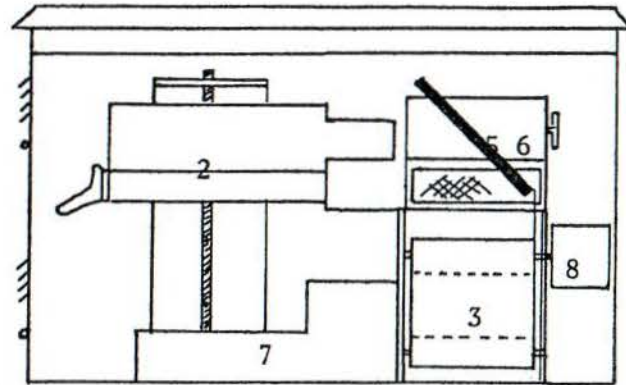
The types of crystals reaching the ground were also determined by using Schaefer's formvar replicating technique (1964) and supplemented by visual observations of the crystals collected on a black velvet snow board. The formvar replicas were produced by exposing microscope slides and 4 inch by 4 inch glass slides, which were covered



INDEX

1. collection area
2. camera
3. felt belt
4. dry ice trays
5. front surface mirror
6. strobe
7. electronics area
8. motor

front 1/6 scale



1/12 scale

side 1/6 scale

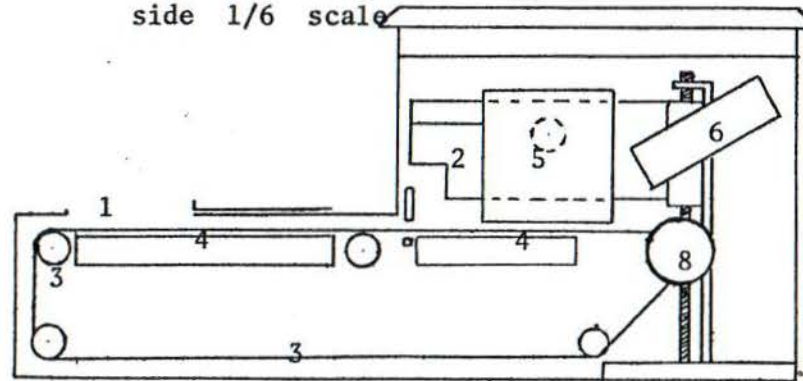


Fig 3 Snow crystal camera

with a 1% solution of formvar and ethylene dichloride, to the falling snow. These slides were then stored in a cooled chamber with dessicating material. The hardened replicas were then examined under a microscope (10x - 70x) using oblique lighting.

## 4. Data Analysis

### 4.1 Transmissometer snow data

The signal voltage output ( $E_t$ ) of the sensor was first averaged over a fifty second time interval, by eye, from the strip charts. The background voltage ( $E_b$ ) was determined for a ten second period every minute during which the shutter assembly closed, thus preventing the signal lamp light from reaching the receiver. These voltages were then transformed to their corresponding intensities and subtracted to give the signal intensity ( $I_s$ ). Using a previously determined reference signal intensity ( $I_o$ ) and Beers law, the extinction coefficient was determined for this time interval:

$$I_s = I_o \exp(-\sigma x) \quad \text{or} \quad \sigma = -\frac{1}{x} \ln\left(\frac{I_s}{I_o}\right) . \quad (1)$$

An average clear air visibility determined from periodic AEG readings was used to determine the extinction coefficient ( $\sigma_c$ ) due to aerosols, humidity, and extremely small hydrometeors via the Koschmieder formula. These clear air extinction coefficients were subtracted from the transmissometer extinction coefficients ( $\sigma_T$ ) to give the extinction coefficients due solely to precipitable size hydrometeors ( $\sigma_p$ ). These  $\sigma_p$  values were then used to calculate visibilities via the Koschmieder formula, and attenuation coefficients ( $k$ ) for each time interval, as follows:

$$V = \frac{3.912}{\sigma_p} \quad \text{Koschmieder (1924)}$$

$$I_s = I_o \exp(-\sigma x)$$

$$\ln\left(\frac{I_s}{I_o}\right) = -\sigma x$$

$$\log\left(\frac{I_s}{I_o}\right) = .434 \ln\left(\frac{I_s}{I_o}\right) \quad (2)$$

$$10 \log\left(\frac{I_s}{I_o}\right) = -4.34 \sigma x$$

$$k = \frac{1}{x} 10 \log\left(\frac{I_s}{I_o}\right) = -4.34 \sigma$$

The attenuation coefficient was then weighted by the precipitation rate (melt water) over suitable time intervals. This precipitation was determined by averaging the two weighing buckets' catch and the one heated tipping bucket on the roof's readings. A computer program was developed to aid in the data reduction. It computed the visibilities in "snow only," and the observed visibilities, as well as the corresponding attenuation parameters. The program also averaged the calculated values and yielded the melt water precipitation rate. Sample computer output is shown in Figure 4.

#### 4.2 Rain data

It was decided that for the spring and early summer rainfall we would invert Atlas' theoretical and empirically averaged visibility-rainfall rate relationships to express rainfall rate as a function of visibility. One could thereby investigate the concept of measuring rainfall rate optically. Here his assumed threshold contrast of



VISIBILITY	EXTINCTION COEF	ATTENUATION COEF	AS OBSERVED	EXTINCTION COEF	ATTENUATION COEF	INTENSITY
2.949	1.3268	5.74	1.169	2.6772	11.63	5.1480
3.790	1.0321	4.48	1.249	2.5053	10.88	5.2735
3.790	1.0321	4.48	1.249	2.5053	10.88	5.2735
2.017	1.9399	8.43	.917	3.4132	14.82	4.7399
2.690	1.4544	6.32	.999	3.1308	13.60	4.8998
2.690	1.4544	6.32	.999	3.1308	13.60	4.8998
2.420	1.6145	7.02	.980	3.2929	14.30	4.8074
THE FOLLOWING VALUES ARE AVERAGED OVER 54.0 MINS						
3.772	1.0371	4.50	1.043	2.1880	9.42	4.8074
IN SNOW ONLY AVG ATT COEF DB/KM/MM-HR = 17.5733						
AS OBSERVED AVG ATT COEF DB/KM/MM-HR = 37.070						
PRECIPITATION RATE = .254MM/HR						
2.602	1.5033	6.53	.928	3.3732	14.65	4.7622
2.410	1.6229	7.05	.896	3.4928	15.17	4.4958
2.915	1.3423	5.83	.974	3.2121	13.95	4.8532
THE FOLLOWING VALUES ARE AVERAGED OVER 10.0 MINS						
2.731	1.4325	6.22	1.018	3.0734	13.35	4.8532
3.327	1.1740	5.11	1.013	3.0900	13.42	4.9233
2.637	1.3789	5.99	.950	3.2929	14.30	4.8074
2.478	1.5788	6.84	.896	3.4928	15.17	4.4958
2.262	1.7295	7.51	.848	3.6898	16.02	4.5883
2.369	1.6510	7.17	.864	3.6113	15.68	4.6308
2.262	1.7295	7.51	.848	3.6898	16.02	4.5883
2.441	1.6024	6.94	.846	3.6113	15.68	4.6308
2.004	1.9521	8.48	.790	3.9411	17.20	4.4444
1.892	2.0477	8.98	.768	4.0744	17.70	4.3844
2.038	1.9192	8.34	.790	3.9411	17.20	4.4444
THE FOLLOWING VALUES ARE AVERAGED OVER 10.0 MINS						
2.331	1.6785	7.29	.858	3.6478	15.84	4.4439
2.123	1.8423	8.00	.805	3.8850	16.87	4.1843
2.694	1.4509	6.30	.896	3.4928	15.17	4.4953
2.648	1.4772	6.42	.876	3.5727	15.52	4.4518
2.798	1.3981	6.07	.896	3.4928	15.17	4.4953
2.648	1.4772	6.42	.876	3.5727	15.52	4.4518
2.792	1.4009	6.08	.886	3.5332	15.34	4.4735
2.714	1.4405	6.26	.876	3.5727	15.52	4.4518
2.714	1.4405	6.26	.876	3.5727	15.52	4.4518
2.642	1.4808	6.43	.848	3.6704	16.03	4.5878
2.642	1.4808	6.43	.848	3.6704	16.03	4.5878
THE FOLLOWING VALUES ARE AVERAGED OVER 10.0 MINS						
2.627	1.5889	6.97	.847	3.6078	15.67	4.5878

Fig 4 Sample output from computer program which analyzed transmissionmeter voltages and clear air visibilities for extinction and attenuation coefficients

$\epsilon = .055$  was maintained to allow direct usage of aviation visual range and airport transmissometer readings. The relationship theoretically derived is  $R = (.104 V)^{-1.49}$  and the empirically adjusted relationship is  $R = (.086 V)^{-1.58}$ .

Visual range and hourly precipitation data were taken from the National Weather Service station at Albany Airport. An hourly average visual range was determined and was used to calculate precipitation rate. The observed precipitation rate was determined by using an hourly accumulated precipitation which was assumed to fall uniformly over the entire hour. This observed rate and the calculated rate were then compared.

## 5. Precipitation Characteristics

### 5.1 February 16, 1973 snow characteristics

The snow crystal type of the February 16 storm was somewhat unusual. National Weather Service data for February 16 shows a total of 0.18 in (4.6 mm) of melt with 6.8 in (17.3 mm) of snow depth. Similar results were observed at SUNY-A snow stations, with a melt water accumulation of 0.09 inches for the 0840 to 2040 twelve hour observation period (during this period Albany Airport reported 0.14 in (3.6 mm) melt and 5.7 in (14.5 cm) snow, a snow depth-melt water ratio of 41 to 1), and a snow accumulation of approximately 2 1/2 inches. This corresponds to a snow-melt ratio of approximately 28 to 1. The National Weather Service data snow-melt ratio was approximately 38 to 1. These ratios are all high compared to the average accepted ratio of 10 to 1. A conclusion is that the snow consisted of flakes with a very open structure, in accordance with the classification of Jiusto and Kaplan (1972).

The snow crystal type started out (0950L)\* as mainly stellar crystals in large aggregates, sometimes with columns growing along the C-axis. Around 1010 hours the crystal type changed to single stellar and sector crystals, usually small, but some as large as 5 mm. But within a few minutes the crystals were observed to again aggregate, with small stellar crystals predominant in these aggregates. This general trend continued through 1200 hours. But a closer examination

---

\*All times are local.



at 1107 and 1150L showed a large variety of crystal types with double capped columns, sectors, plate assemblages, pyramids and planar dendritic crystals all present. The plate assemblages and dendritic fragments proved to be the predominant types through this time period. The number of aggregates observed decreased towards 1200 and fluctuated to about 1440 hours, with peaks at about 1210 and 1300. These aggregates again were predominantly stellar crystals with some columns. Very small plates, planar dendrites, double capped columns, and a mixture of the plate and dendritic growth modes became mixed with larger aggregates from about 1200 hours. They completely dominated the observed crystal structure by 1440, when aggregates were no longer observed. From this time forward, the crystals were very small, sometimes too small ( $d < .1$  mm) to recognize without a microscope. They consisted mostly of fragments and irregular crystals. The experiment ended at 1615 due to an electronic malfunction in the receiver. However, crystal observation until 1745 showed an increasing trend towards small crystals, mainly hexagonal plates. It was after this period that the accumulated melt water reached a one hour peak of 0.04 in (1.0 mm) reported at the Albany Airport. No such increase was observed at SUNY-A snow stations, which continued to record precipitation through the night.

#### 5.2 February 22, 1973 snow characteristics

The snow crystal type of the February 22 storm was predominantly heavily rimed crystals and flakes. The National Weather Service data for the February 21-22 storm showed a total estimated (due to melting) snowfall of 0.7 in (17.8 mm) with a melt water accumulation of



0.08 in (2.03 mm). At SUNY-A the total snowfall was estimated as 0.55 in (14.0 mm) with a melt water accumulation of 0.055 in (1.40 mm). Because these are only estimates of snowfall, no snow-melt ratio could be determined. A conclusion is that the snow was mainly wet and perhaps the flakes were even partially melted when they reached the surface.

The observations began at 1950 hours, when the precipitation was an ice-rain mixture. As the storm continued, liquid water was observed in decreasing amounts. By 2022L raindrops were observed sporadically, and by 2047 all the precipitation was in the form of wet irregular ice chunks, some showing riming. Crystals first became recognizable around 2130, but they were so heavily rimed as to prevent type identification. Around 2200 the riming had decreased to an extent that aggregates could be defined; however, the riming was still too heavy to identify crystals. The riming intensified shortly after the observation, so that at 2230 no shapes of the heavily rimed crystals were apparent. The crystal type could be determined by 2305 when the riming decreased. The crystals were predominantly dendrites and stellars, and the aggregates were formed of spacial dendrites, stellars, and sectors. The amount of water available, or a warm layer above again caused the crystals to turn into dry ice pellets around 2330, but by 0010 crystal type could again be determined to be plate assemblages, sectors, and spacial dendrites. From this point in the storm until the end of the data taking period (0310) the crystal type could be determined. At 0040L columns, capped columns, and hexagonal plates predominated the crystal form. This continued to 0100 when sectors and irregulars replaced columns and capped columns. Shortly thereafter (0110) heavily rimed

plate assemblages and sectors were observed. Then at 0115 the crystals became very small and by the last observation (0140) very few aggregates with some stellars and irregulars were observed among the more numerous small crystals or fragments.

## 6. Discussion

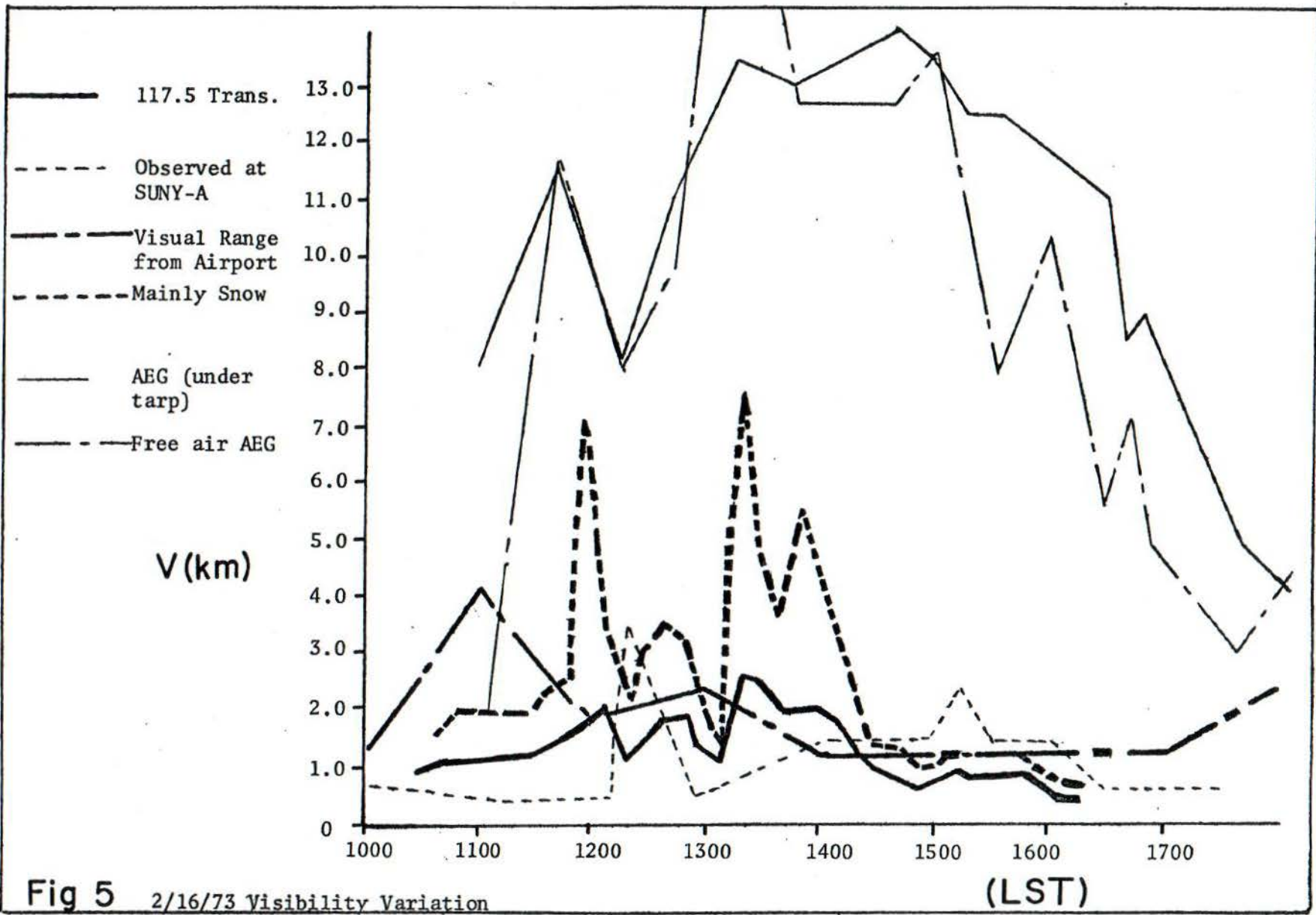
### 6.1 February 16 storm

The attenuation coefficient variation during the February 16 snow storm shows some interesting variations if we divide the storm up into three periods: 1) aggregates (snowflakes) dominated period (1030 - 1130L); 2) transition period from aggregates to single crystals (1130 - 1440); and 3) single crystal dominated period (1440 - 1615).

During the first period the attenuation coefficient for snow exclusively averaged between 14.1 and 4.1 db km<sup>-1</sup> with relatively high melt water rates of 0.177 mmw hr<sup>-1</sup> and 0.127 mmw hr<sup>-1</sup>. The first of these rates is a 30 minute average (1030 - 1100) totally in the aggregate dominated period. The second rate is a 60 minute average (1100 - 1200) where half the average interval lies in the aggregate period and half in the transition period. The observed attenuation coefficient varied in the same manner as the attenuation coefficient for "snow only," with the difference roughly averaging out to be 2 db km<sup>-1</sup>. As we approach the transition period the attenuation coefficient begins to drop. The high peaks of the attenuation coefficient (low visibility) during the transition period correspond to periods where aggregates were observed to increase in number. See Figure 5, in particular time periods 1218, 1258, and 1308.

In Figures 5 and 6 are plotted visibility variations during the experiment. Shown on these graphs are: 1) the visibility as observed by the transmissometer without the "clear air" visibility correction; 2) the visibility as physically observed by the author; 3) the visual







range recorded at Albany Airport by the official observer (when the visual range dropped below 3.2 km, the airport transmissometer was used to determine the visual range); 4) the visibility as calculated by the SUNY-A transmissometer with the clear air visibility corrections (that is the transmissometer minus the AEG "under-tarp" visibility); 5) the visibility recorded by the sheltered AEG; and 6) the visibility recorded by the AEG exposed to the air flow.

The precipitation (melt water) rate observed during the transition period was relatively low ( $0.063 \text{ mmw hr}^{-1}$ ). This rate was observed over two 58 minute sample times. As the transition period ended, the attenuation coefficient for "snow only" increased and the difference between the snow only coefficient and the observed coefficient decreased to approximately  $1.25 \text{ db km}^{-1}$ . The precipitation rate during the latter part of the transition period and the early single crystal period was observed at  $0.127 \text{ mmw hr}^{-1}$ . During the single crystal period the attenuation coefficient reached its highest levels. The maximum attenuation coefficient was recorded during the period when the crystals were their smallest in size. This occurred during the last nine minutes of operation. The precipitation rate for this single crystal period was again relatively low ( $.063 \text{ mm hr}^{-1}$ ). This is a 60 minute averaged precipitation rate. The average attenuation coefficients for the entire storm were  $9.07 \text{ db km}^{-1}$  in "snow only," and  $10.5 \text{ db km}^{-1}$  as observed. Variations in all optical and precipitation variables during the storm are detailed in Table 1..

## 6.2 February 21-22 storm

The February 21-22 storm was an unusual storm in that it exhibited different precipitation and weather types. The storm could

TABLE I  
Average Data Summary

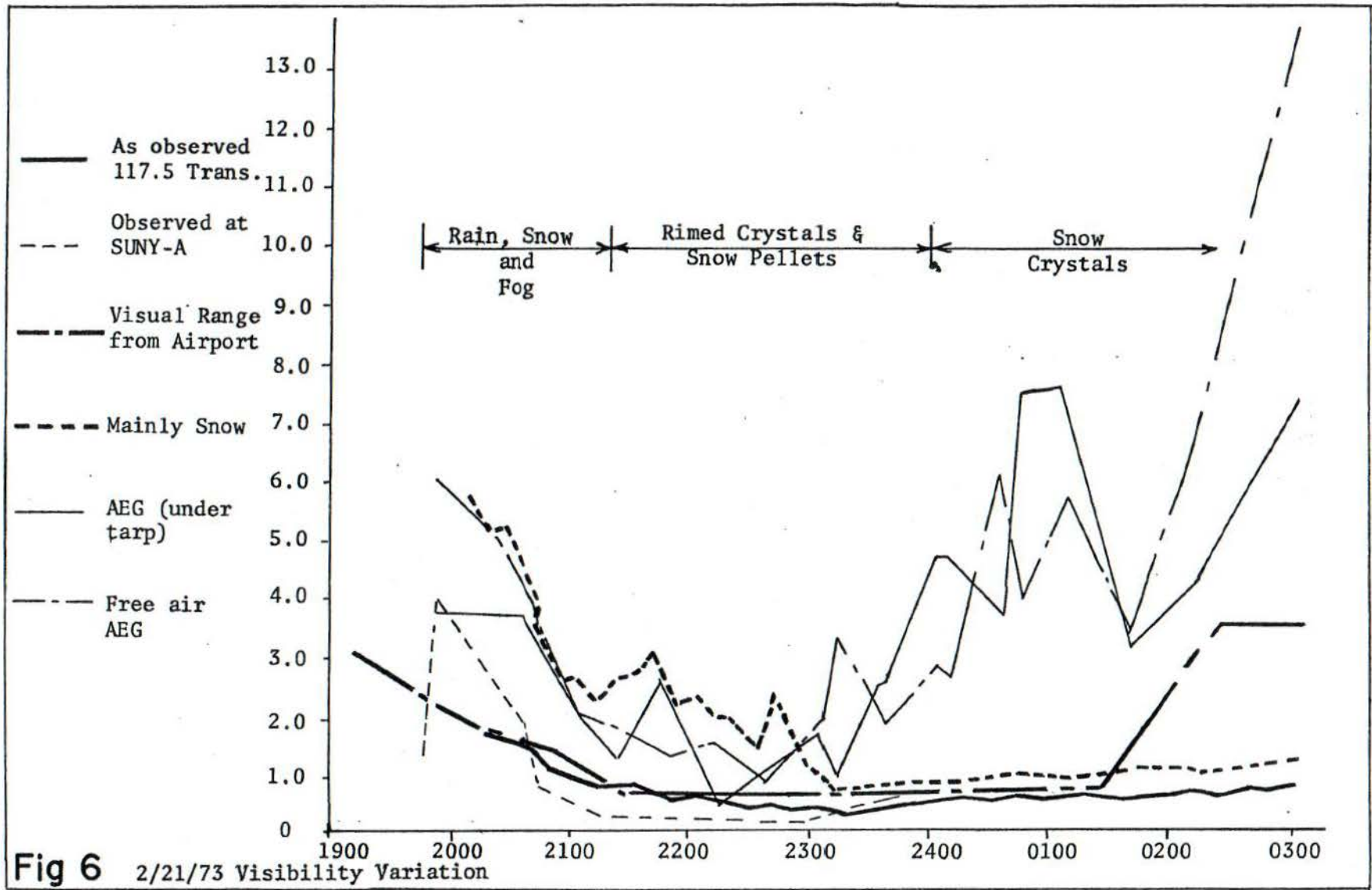
Date	Time Interval Ending	Time Averaging Interval (min.)	As Observed			Snow Only			R mmwhr <sup>-1</sup>
			V (km.)	$\sigma$ (km <sup>-1</sup> )	k (db km <sup>-1</sup> )	V (km.)	$\sigma$ (km <sup>-1</sup> )	k (db km <sup>-1</sup> )	
2/16/73	10:56	33	1.229	2.5462	11.06	1.092	2.0572	8.93	.177
	11:56	60	1.658	1.8877	8.20	2.636	1.4843	6.45	.127
	12:58	58	1.736	1.8026	7.83	2.782	1.4062	6.11	.063
	13:50	58	2.315	1.3517	5.87	3.714	1.0533	4.57	.063
	14:52	58	1.081	2.8949	12.57	1.500	2.6079	11.33	.127
	15:52	60	0.878	3.5643	15.48	1.202	3.2536	14.13	.063
2/21/73	20:59	54	1.443	2.1680	9.42	3.772	1.0371	4.50	.254
	21:59	60	0.801	3.9082	16.97	2.514	1.5560	6.76	.063
	22:59	60	0.570	5.4921	23.85	1.676	2.3342	10.14	.381
	23:59	60	0.516	6.0616	26.33	0.876	4.4662	19.40	.254
2/22/73	00:59	60	0.677	4.6216	20.07	1.041	3.7565	16.31	.190
	01:59	60	0.708	4.4173	19.18	1.096	3.5698	15.50	.127
	02:59	60	0.765	4.0877	17.75	1.174	3.3308	14.47	.127



be divided up into three periods. The first period was the rain, snow and fog mixture period which existed at the start of the data period, 1957L, and continued to about 2115 when crystals first became recognizable. At 2105 Albany Airport reported the rain as stopping, and at the same time the fog started to decrease at SUNY-A. The second period was the snow only period, which started around 2130, when Albany Airport reported only snow falling. This period ended somewhere between 2330 and 0010 (2/22/73), during which time dry ice pellets were observed to predominate the hydrometeor forms. The third period began around 0010, when ice crystal type could again be determined. Also at 0015, Albany Airport, 6.4 km NNE of SUNY-A, reported a snow-fog mixture. This continued until the end of the data period (0310).

The attenuation coefficient for "snow only" increased, as one would suspect (Figure 6), as the precipitation changed from rain to heavily rimed snow crystals and ice pellets. It is interesting to note that as the fog was clearing around 2105 the patchiness of the dispersing fog is evident in fluctuations of the attenuation coefficient from a one minute average high of  $8.98 \text{ db km}^{-1}$  to a low one-minute average of  $5.11 \text{ db km}^{-1}$ . The fluctuation in general raised the ten minute average  $k$  to a relatively high peak of  $7.29 \text{ db km}^{-1}$ . As the fog continued to clear, the attenuation coefficient dropped, but this is not the only reason for the decrease. The precipitation rate also decreased from  $.254 \text{ mmw hr}^{-1}$  (a 54 minute average ending at 2052) to  $.063 \text{ mmw hr}^{-1}$  (a 60 minute average ending at 2152). The snow crystals were observed during the second period (2200-2300L) to be heavily rimed aggregates and crystals, mostly rimed beyond recognition. The precipitation rate in millimeters of melted water per hour was observed





at SUNY-A to be  $0.381 \text{ mmw hr}^{-1}$  and at Albany Airport to be  $0.508 \text{ mmw hr}^{-1}$ . This could account for an increase in the attenuation coefficient, as well as a change in the type of scatterers. In the 2300-2400 time interval the crystal type changed to aggregate and spacial dendrite in particular. These crystals, with their large scattering area and open structure produced a smaller precipitation (melt) rate with a high attenuation. These crystals and flakes gave the largest attenuation coefficient measured. The precipitation rate was measured to be  $0.254 \text{ mmw hr}^{-1}$ . During the third period, the crystals changed to the smaller scattering area type, namely, columns and hexagonal plates. This had occurred by 0040. This change in crystal type, coupled with a decrease in the precipitation rate to  $0.190 \text{ mmw hr}^{-1}$ , offset the effects of the fog and decreased the attenuation coefficient. The precipitation was recorded at a constant rate of  $.127 \text{ mmw hr}^{-1}$  from 0100 to 0300L. During the final phase of data taking, the crystals changed to very small and irregular types. The attenuation coefficient gradually decreased to  $12.8 \text{ db km}^{-1}$  in moderate fog and very light snow. The average attenuation coefficients for the whole storm were  $12.5 \text{ db km}^{-1}$  for snow only, and  $19.0 \text{ db km}^{-1}$  as observed.

### 6.3 Sample volume

During the winter data-taking period an additional AEG/Telefunken light scattering meter was exposed to the natural air flow of the snow-storm on a ledge approximately two meters above the roof level near the instrument hut. This was done to examine the usefulness of an optical instrument of small sample volume for accurate visibility and precipitation rate determinations. The visibility determined by the AEG unit was compared with the visibility determined by the adjacent 117.5 m

base-line transmissometer; the visual range as reported by the National Weather Service station at Albany Airport 6.4 km NNE of SUNY-A; the sheltered AEG 5 m away; and the visual observations of the maximum visibility made by this investigator from the roof. The results are shown in Figures 5 and 6. They show that the visibilities all agree fairly well when fog as well as precipitation is present, as on February 21. However, when fog is not present there are wide discrepancies between the free air AEG readings and the other visibility determinations in free air. The free air visibilities of the AEG agree well with those of the sheltered AEG in foggy conditions (2030-2130 2/21/73). Only as the fog decreased did they separate somewhat, but both remained considerably different from other visibility measurements. In short, the small sample volume ( $7.9 \times 10^{-4} \text{ m}^3$ ) discriminates against the relatively low concentrations of large hydrometeors (snow and rain).

#### 6.4 Spring and summer rains

Although the standard NWS precipitation rate data and visibility data are coarse in their time resolution and averaged over an hour or longer, the agreement between the observed precipitation rate and the calculated precipitation rate (Section 4:2) is very good, as seen in Figure 7. This good agreement is of course limited to rainstorms without fog, and to those where the rain is uniformly spread over the hour. A graphic partial summary of the comparison of the observed rainfall rate  $R$  and computed  $R$  based on visibility measurements in several rainstorms is shown in Figure 8. Clearly, the occurrence of fog with rain degrades any systematic correspondence.



5/8/73

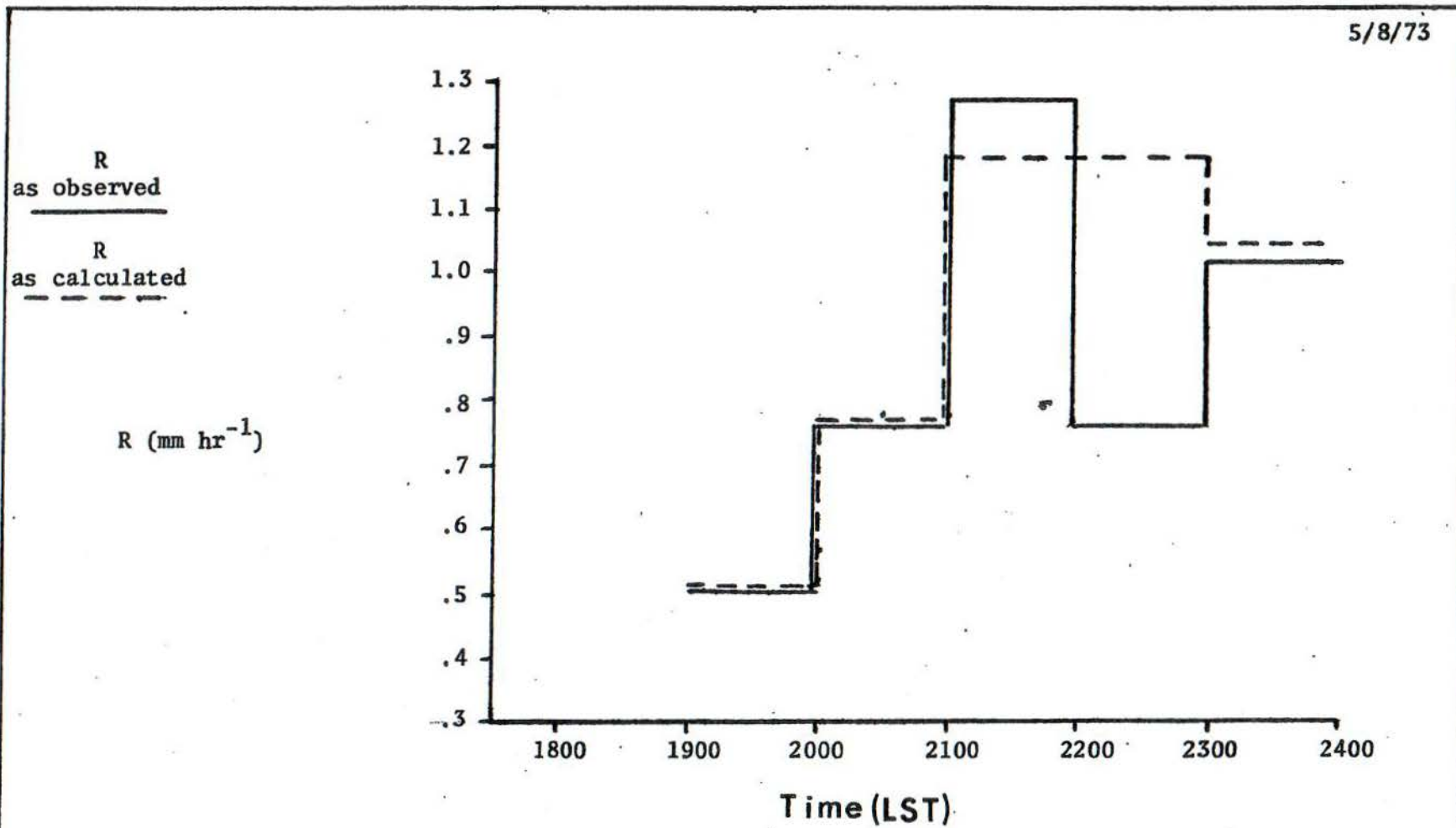
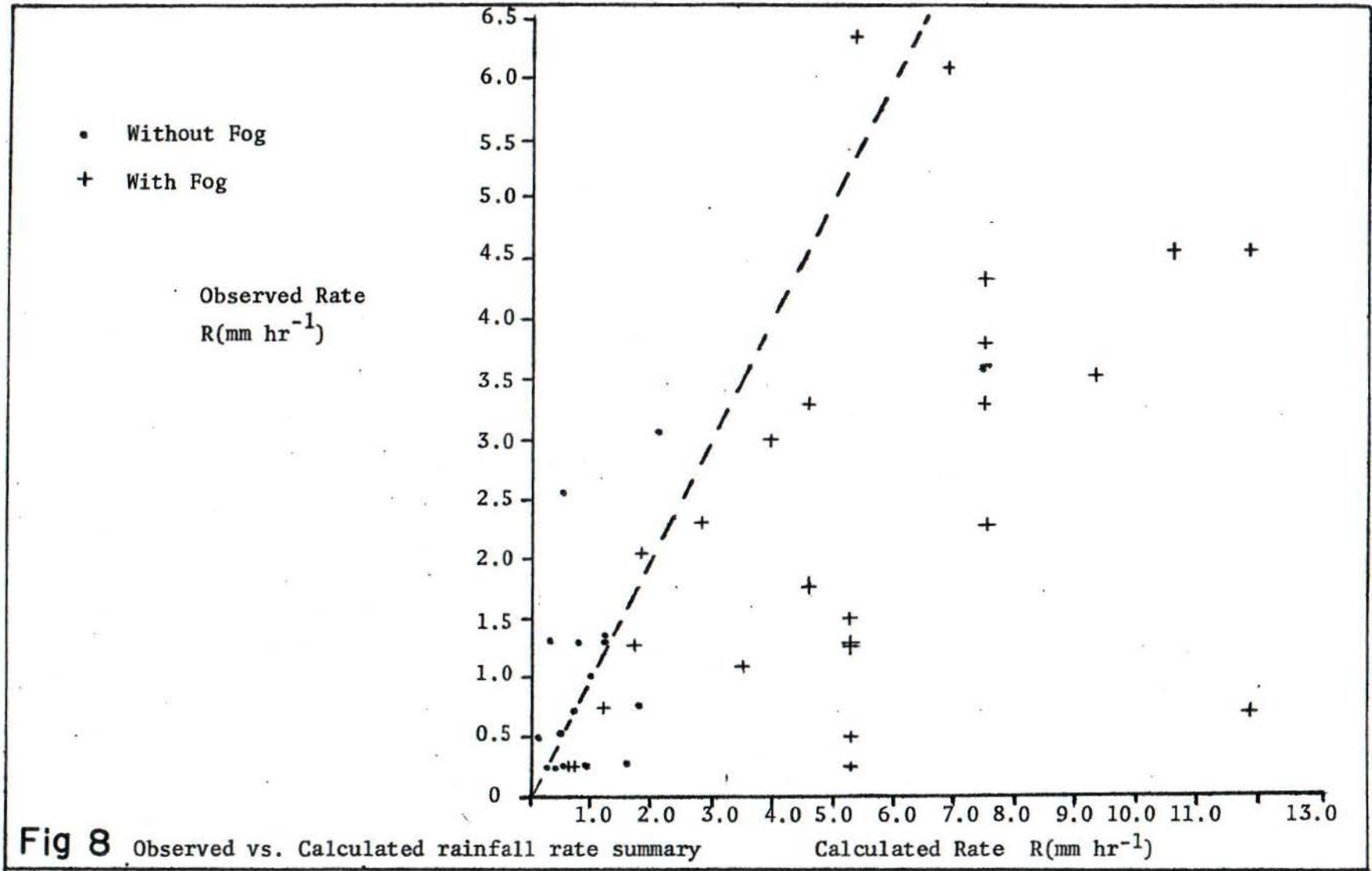


Fig 7 Observed and calculated rainfall rates in a typical no fog case



## 7. Error Analysis

The method whereby the original data were reduced is the first source of possible error. The major trends and fluctuations are not open to doubt, as they were measured on the charts directly; however, small variations of the signal level could have been the result of the second and third decimal place estimates made by use of a scale divided into four 0.025 V sections. The second possible source of error is the clear air visibility readings. Since rapid fluctuations take place in local visibilities, and since the AEG was not sampling any portion of the transmissometer sample volume, and further, was in a position where building heat and restricted airflow could have reduced the immediate local relative humidity and thereby dissipated some of any local fog present, erroneously high clear air visibility could have been recorded. The third possible source of error is the interpretation of the weighing bucket melt precipitation data. This could be due to poor site location. The weighing buckets and tipping bucket were located atop a three story building where, despite Alter windshields, the buckets read low when compared with the National Weather Service readings for these two storms.

Of these three major sources of error I consider none of them to invalidate the results, although they force a limitation on the application of the results. The overall error estimate is  $\pm 40\%$ .



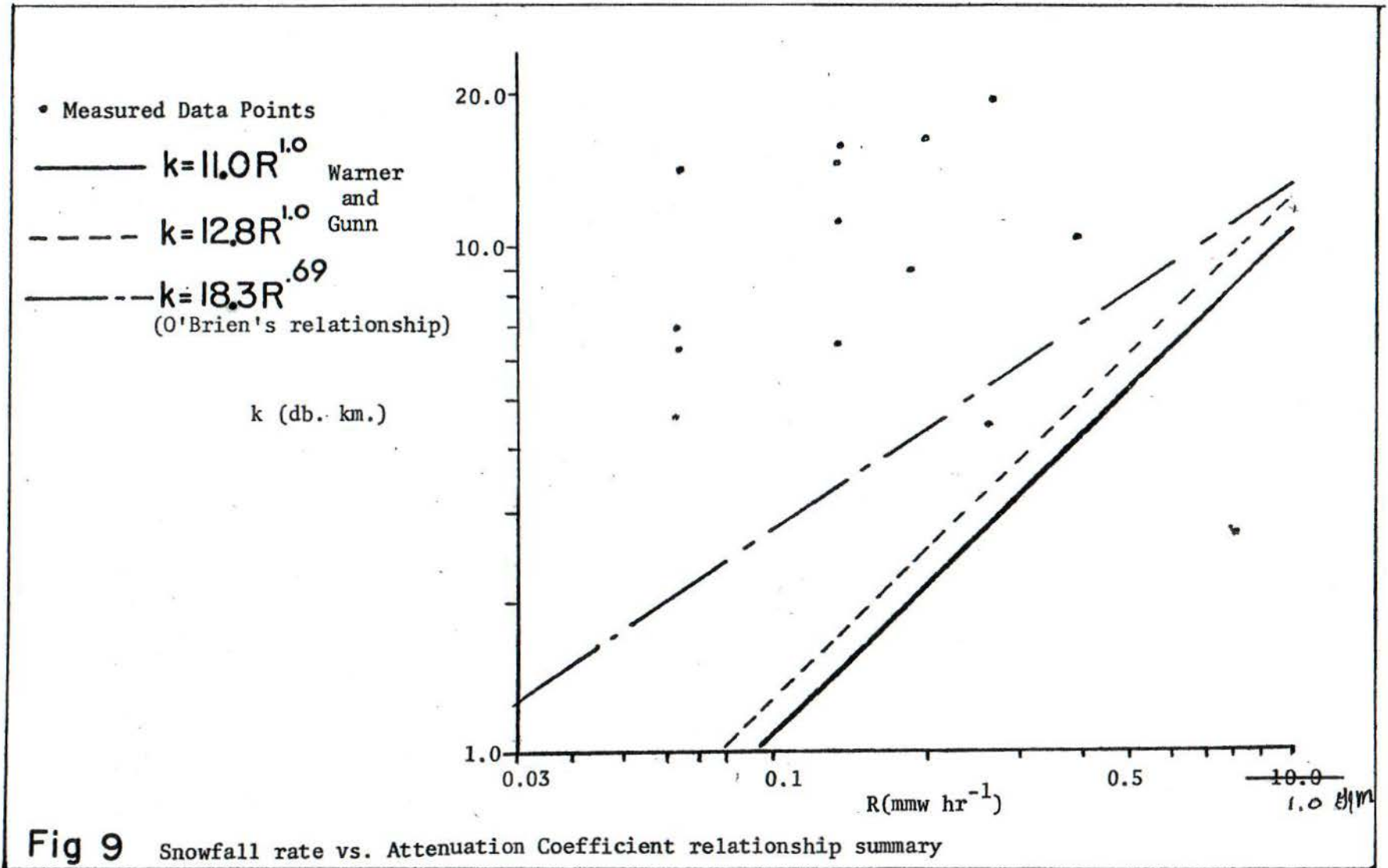
## 8. Conclusions

The results of the winter experiment are shown as plotted points in Figure 9. Also included in the diagram are the curves resulting from Warner and Gunn's (1969) experiments and from O'Brien's (1970) theoretical work.\*

This diagram shows a wide scattering of points. This could be due to erroneous low precipitation catches on the roof or due to the peculiar types of precipitation occurring during the observations. An examination of the actual differences in precipitation catch can account for only part of the observed departure from Warner and Gunn's and O'Brien's work. The conclusions that one draws can be only tentative due to the low sampling time. However, the results do confirm the suggestion of Warner and Gunn that the crystal type is one of the determining factors causing variations in the attenuation coefficient. This fact leads one to believe that local adjustments must be made to any R-k relationship, and that the location of application must consistently receive approximately the same crystal types during the observation period as was experienced during the calibration. Also, the longer the averaging period the more accurately the snowfall rate could be known if the above condition is satisfied. However, this longer averaging partly defeats one of the presumed advantages of optical snowfall rate techniques, namely fine time resolution.

---

\*O'Brien's precipitation measurement, mass flux, has been converted into a precipitation rate  $R$  ( $\text{mm hr}^{-1}$ ).



Aside from these meteorological conditions, the instrumental problems may very well make this technique of measuring precipitation prohibitively expensive as compared to other techniques. Some of these limitations on the feasibility of this technique are experienced by airport transmissometers. The optics and any glass surface exposed to the atmosphere must be heated to prevent condensation. Also, these surfaces must be protected against the collection of precipitation or dirt and dust from the air. The light source must have a minimum output change during its life, or employ a dual beam reference monitor. A new source must be ready to replace the old one without aging, which necessitates multiple recalibration of  $I_0$ . All housings must be firmly erected so as to eliminate wind vibration or shifting of the alignment. The system must be free of any heated buildings and away from regions where high concentrations of plant seeds, pollen, or insects frequently cross the beam. The clear air visibility must be continuously sampled nearby to compensate for attenuation by fog and haze. The sample volume must be large enough to obtain an accurate representation of the scattering medium. The money, time, site restrictions and maintenance necessary to meet all of the requirements of this type of system, in my opinion, cannot be justified when compared to the less demanding requirements and expense of standard precipitation instruments.

More standard rugged visibility instruments such as the AEG light scattering meter would meet most of the requirements for such a system. However, the adequacy of the sample volume is open to question. This limited series of experiments has shown that the sample volume of the AEG is much too small to be used to determine visibility in snowfall.



As one turns to precipitation measurement in rain, the optical idea approaches feasibility. It is clear that no elaborate local adjustments are necessary to the R-V relationship. This was tentatively shown by our experiments, as the agreement with Atlas' relationship was good. If clear air visibility could be continuously measured and used with an accurately calibrated runway transmissometer, local precipitation could be determined.

The final conclusion is that the meteorologically and technically imposed limitations made the optical method of determining precipitation rate, as investigated, unfeasible for widespread application. For research purposes, where great care can be taken with instrumentation details and specification of the precipitation scatterers, it may be quite useful.

## REFERENCES

- Atlas, D., 1953: Optical extinction by rainfall. Journal of Meteorology, vol. 10, no. 6, 486-488.
- aufm Kampe, H., and H. Weickmann, 1952: Trabert's formula and the determination of water content in clouds. Journal of Meteorology, vol. 9, no. 3, 167-171.
- Cornford, S., 1967: Sampling errors in measurements of raindrop and cloud droplet concentrations. Meteorological Magazine, vol. 96, 271-282.
- Horvath, H. and K. Noll, 1969: The relationship between atmospheric light scattering coefficient and visibility. Atmospheric Environment, vol. 3, no. 41, 543-550.
- Jiusto, J. and M. Kaplan, 1972: Snowfall from lake-effect storms. Monthly Weather Review, vol. 100, no. 1, 62-66.
- Johnson, J., 1954: Physical Meteorology. Massachusetts Institute of Technology, pp. 69-99.
- Koschmieder, H., 1924: Theorie der horizontalen sichtweite. Phys. freien Atmos., 12, 33-55, 171-181.
- Lillesaeter, O., 1965: Parallel-beam attenuation of light, particularly by falling snow. Journal of Applied Meteorology, vol. 4, no. 5 607-613.
- Magono, C. and C. Lee, 1966: Meteorological classification of natural snow crystals. Journal of the Faculty of Science, Hokkaido University, Series VII (Geophysics), vol. 2, no. 4, 321-363.
- Marshall, J. and W. Palmer, 1948: The distribution of raindrops with size. Journal of Meteorology, vol. 5, no. 4, 165-166.
- Middleton, W., 1958: Vision Through the Atmosphere. University of Toronto Press, pp. 103-122.
- O'Brien, H., 1970: Visibility and light attenuation in falling snow. Journal of Applied Meteorology, vol. 9, no. 4, 671-683.
- Oddie, G., 1968: The transmissometer. Weather, vol. 23, no. 11, 446-455.
- Philbrick Researches Inc., 1966: Applications Manual for Computing Amplifiers. Nimrod Press, Inc., Section III.80.

Schaefer, V., 1964: Preparation of permanent replicas of snow, frost and ice. Weatherwise, vol. 17, no. 6, pp. 279-287.

Warner, C. and K. Gunn, 1969: Measurement of snowfall by optical attenuation. Journal of Applied Meteorology, vol. 8, no. 1, 110-121.



**APPENDICES**

## APPENDIX I

### List of symbols

$d$	diameter of scattering particle
$\lambda$	wavelength
$\alpha$	$= 2\pi\lambda/d$ scattering parameter
$\sigma$	extinction coefficient
$V$	meteorological range
$\rho$	density of the scattering material
mm w	melted water in millimeters
$W$	liquid water content per unit volume
$L$	local time
$N_i$	number of drops or particles in the $i^{\text{th}}$ category
$r_i$	radius of the drop in the $i^{\text{th}}$ category
$R$	rainfall rate
$D_0$	median volume diameter
$B$	brightness of the background
$\Delta B$	the difference between the brightness of the target and that of the background
$\epsilon$	threshold contrast
$E_T$	raw signal voltage output of the sensor unit
$E_0$	background voltage output of the sensor unit
$I_s$	signal intensity
$I_0$	reference signal intensity
$x$	pathlength
$\sigma_c$	clean air extinction coefficient

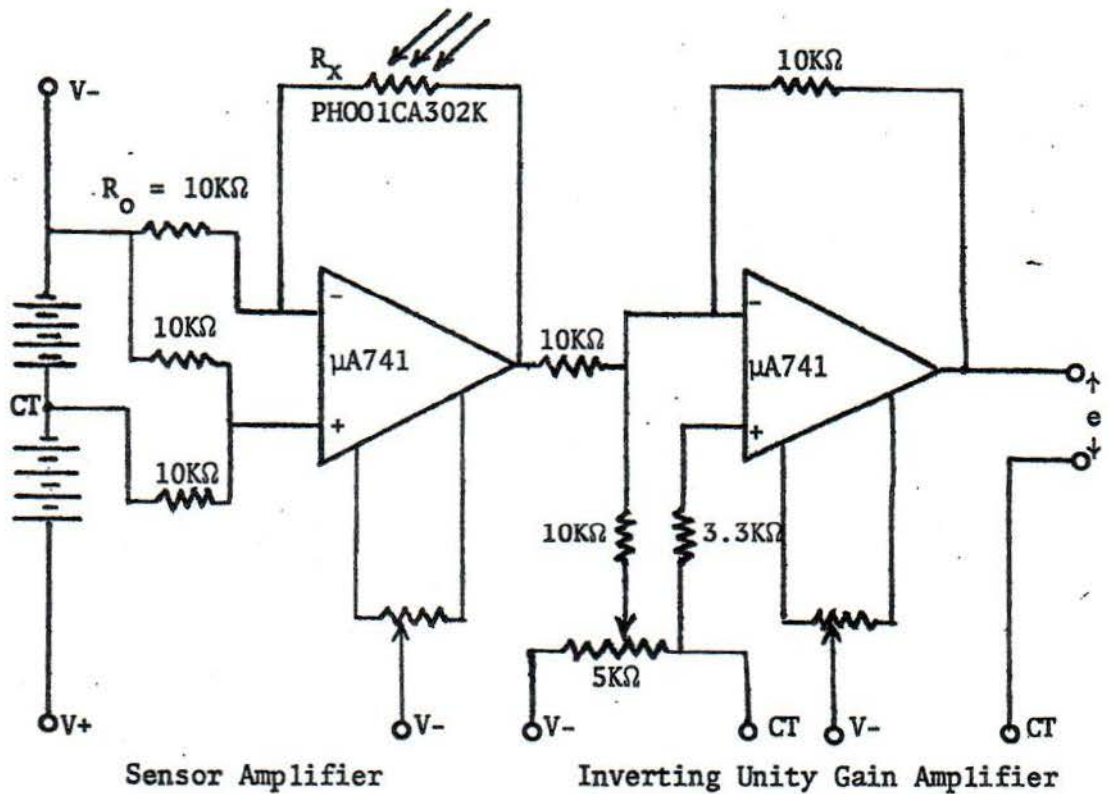
## List of symbols (Cont'd.)

$\sigma_T$	transmissometer extinction coefficient
$\sigma_p$	extinction coefficient due solely to precipitable size hydro- meteors
$k$	attenuation coefficient
$F$	monochromatic light flux at some distance $x$
$F_0$	monochromatic light flux at zero distance
$K_i(\lambda)$	scattering area ratio at the wavelength $\lambda$ and for the particle in the $i^{\text{th}}$ category
$A_i$	geometric cross section of a particle in the $i^{\text{th}}$ category
$e$	amplifier output
$E_0$	half the voltage source
$R_x$	resistance of the photoresistor
$R_0$	bias resistance
$m$	straight line slope
$B$	y intercept at log 1



## APPENDIX II

This detector amplifier circuit was taken from circuit II-1, 2-1 and III-80, 3-80d, Philbrick Researches, Inc. Applications Manual for Computing Amplifiers.



$$e = \beta E_o \quad (1)$$

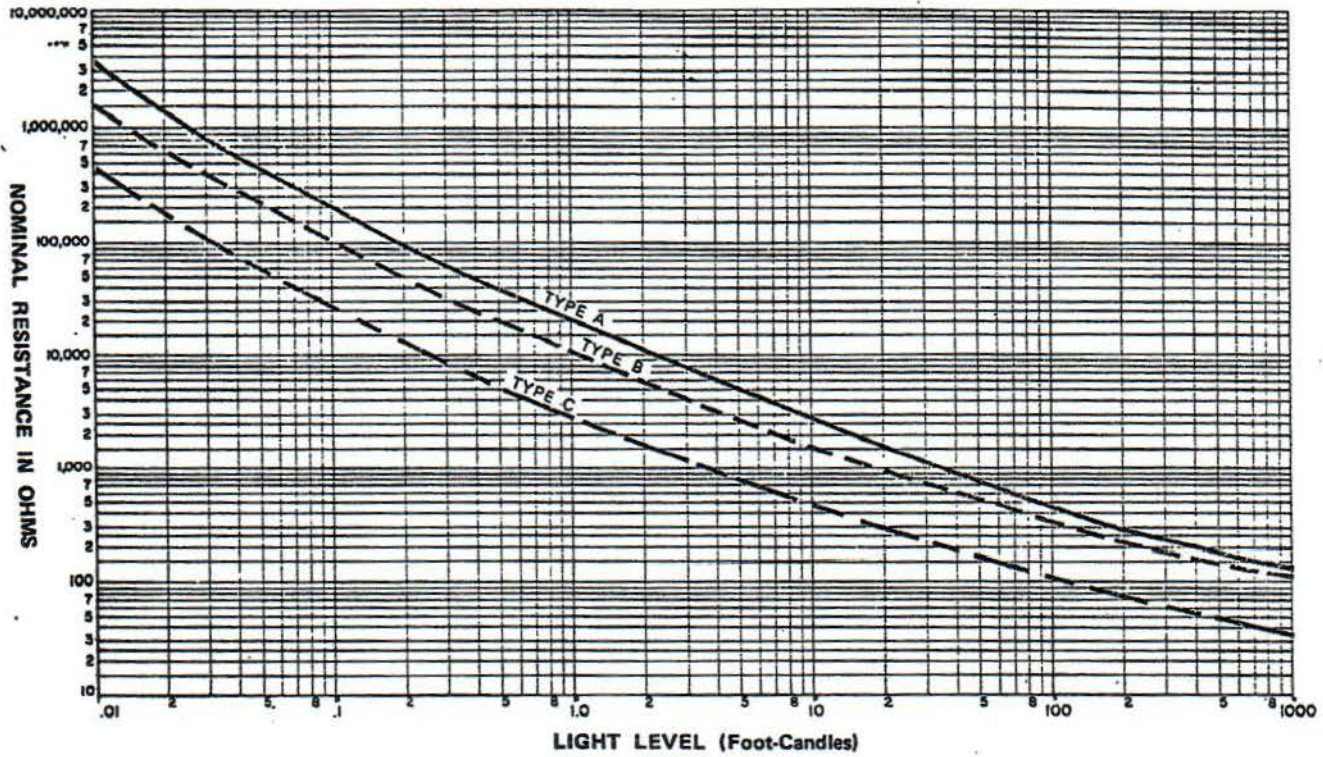
$$\beta = e/E_o$$

$$R_x = R_o(1 + \beta) \quad (2)$$

$$\beta = (R_x/R_o) - 1$$

$$R_x = R_o \left( \frac{e}{E_o} + 1 \right) \quad (3)$$

## RESISTANCE VS. ILLUMINATION



The response curve above for the PH001CA302K photo resistor was approximated by four straight lines.

$$\log R_x = m \log I + \log B \quad (4)$$

$$R_x = BI^m \quad (5)$$

$$I = \sqrt[m]{\frac{R_x}{B}} \quad (6)$$

Resistance Range ( $\times 10^3 \Omega$ )	m	B ( $\Omega$ )	Intensity Range (ft-cd)
1.5 - 11	- .8653	20,039	20 - 2
11 - 49	- .9283	20,933	2 - .4
49 - 95	- .9548	20,429	.4 - .2
95 - 800	-1.3241	11,278	.2 - .04

Combining equations 3 and 5 we get the intensity output voltage relationship.

$$I = \sqrt{\frac{m R_o \left( \frac{e}{E_o} + 1 \right)}{B}} \quad (7)$$



### APPENDIX III

#### Theory of Attenuation

Following the treatment of Middleton (1952, p. 12-13), one may express the flux of a parallel monochromatic light beam at a distance  $x$  from an origin as  $F = F_0 e^{-\sigma x}$  where  $F_0$  is the flux at the origin and  $\sigma$  is the extinction coefficient. The extinction coefficient is composed of a scattering coefficient and an absorption coefficient. The scattering coefficient may be expressed as the sum of the effective scattering cross sections of all the particles in a unit volume of the beam (this assumes a homogeneous scattering medium). Thus,  $\sigma$  may be expressed as  $\sigma = \sum_{i=1}^n N_i K_i(\lambda) A_i$  where  $K_i(\lambda)$  is the scattering area ratio,  $A_i$  is the geometrical cross section, and  $N_i$  is the concentration of particles unit volume. If we restrict ourselves to large values of  $\alpha$  ( $\alpha \geq 200$ ),  $K_i$  becomes a constant equal to approximately 2. Sigma is now almost independent of wavelength. Thus, we can treat a variety of attenuators (snow, fog, rain, etc.) in a relatively simple manner as long as we restrict ourselves to the large  $\alpha$  region.

Another parameter which is often used to describe attenuation is the attenuation coefficient. It can be related to the extinction coefficient as outlined below:

$$F = F_0 \exp(-\sigma x)$$

$$\ln \frac{F}{F_0} = -\sigma x$$

$$\log \left( \frac{F}{F_0} \right) = -.4343 \sigma x$$

$$k = - \frac{10}{x} \log \left( \frac{F}{F_0} \right) = 4.343 \sigma$$

$$k = 4.343 \sigma$$